11 Particle physics with CMS

E. Aguiló, C. Amsler, S. de Visscher, M. Ivova, B. Millán Mejías, P. Otyugova, C. Regenfus, P. Robmann, J. Rochet, T. Rommerskirchen, A. Schmidt, and J. Storey

V. Chiochia, C. Favaro, A. Jaeger, H. Snoek, and M. Verzetti

in collaboration with: Paul Scherrer Institut (PSI) and the CMS Collaboration

After commissioning with cosmic rays the CMS experiment [1] at the LHC recorded proton collisions in December 2009 at the center of mass energy of 900 GeV. The detector performances had to be verified first by comparing with our current knowledge of the standard model. The mass distributions in Fig. 11.2, obtained after various selection cuts, illustrate some of the known particles "rediscovered" by CMS. A run at the unprecedented energy of 7 TeV took place in March – December 2010, collecting about 40 pb^{-1} (see Fig. 11.1). The data analysis of the 2010 dataset is now well advanced. When writing this report, 41 journal articles by the CMS collaboration had been published or were in print. One of us (V.C.) was Deputy Project Manager of the silicon tracker in 2010 and now chairs the B-physics analysis group, that has so far released six journal articles on quarkonium, B mesons and inclusive b-quark production measurements. One of us (H.S.) convenes the pixel calibration and reconstruction group. The silicon pixel detector is the innermost component of the CMS experiment. It allows a precise reconstruction of charged particles and the identification of secondary vertices from long-lived particles. The 53 cm long barrel pixel section, with about 48 million channels, consists of three cylindrical layers at radii between 4.4 cm and

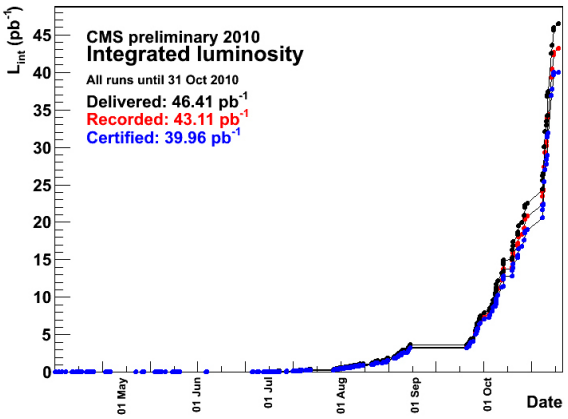

Fig. 11.1 – Integrated luminosity in the 2010 run at $\sqrt{s} = 7$ TeV.

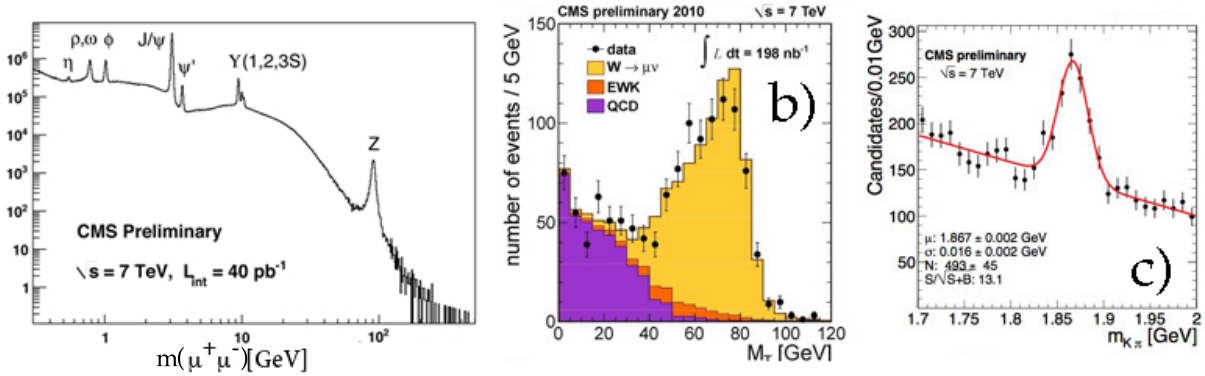

Fig. 11.2 – Some preliminary results obtained during summer 2010: a) $\mu^+\mu^-$ mass distribution showing the vector mesons and the Z^0 peak; b) transverse mass distribution of muons showing the (Jacobian) peak from $W \to \mu\nu$ decay; c) $K^-\pi^+$ mass distribution showing the D^0.

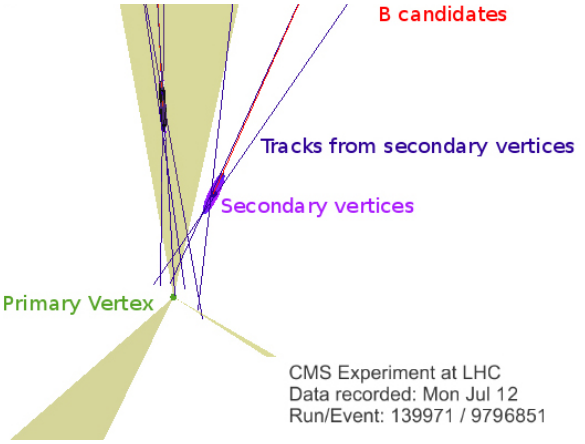

Fig. 11.3 – CMS event showing two displaced vertices from B hadron decays [5].

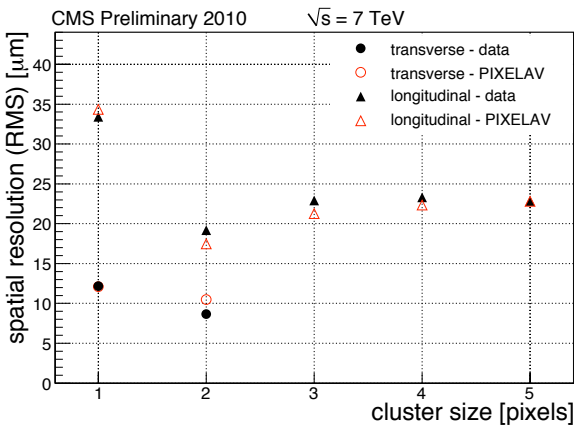

Fig. 11.4 – Transverse and longitudinal hit position resolution of the pixel barrel detector compared to the predictions from PIXELAV simulations.

10.2 cm. Two endcap disks at each side of the barrel section provide coverage up to large rapidities. Details can be found in various publications such as [2–4]. Figure 11.3 shows an event with two displaced vertices from b hadron decays.

11.1 Commissioning of the silicon pixel detector

Our first priority was to measure the pixel detector performance with LHC collisions and to compare with expectations. We performed several important measurements and calibrations, ranging from the detector occupancy to position resolution [6]. The position resolution was improved with the larger data samples collected at $\sqrt{s}$ =7 TeV. The technique was based on pairs of consecutive hits along a trajectory in the overlap region between two adjacent modules within a layer (see last year's annual report). The data were compared to predictions from the detailed PIXELAV simulation [7]. The transverse and longitudinal resolutions are shown in Fig. 11.4 as a function of cluster length. The agreement between data and prediction is remarkable, demonstrating the excellent understanding of the detector response already in the early phase of its operation.

11.2 Improvements to hit and track reconstruction

Searches for the Higgs boson and Supersymmetry depend heavily on the identification of τ leptons and b-quarks. Since the transverse momentum of the τ jet is large compared to the τ mass, the decay pions emerge as collimated jets in which individual tracks become inseparable with increasing momentum. Hits in the pixel sensors merge forming broad clusters (in the inner-most pixel layer when the opening angle between two trajectories is below 5 mrad). For a typical 3-prong τ decay this angle corresponds to a transverse momentum of 150 GeV/c. Hit merging deteriorates the reconstruction of the τ mass, thus excellent spatial resolution is needed for τ reconstruction.

Merged clusters generate peaks in the cluster charge distribution at integer multiples of the minimum ionizing energy deposit. We have therefore developed an algorithm to split the merged cluster. The track impact angle on the sensor is used to compare the observed cluster shapes from the expected ones which were simulated with very high-p_t jets. Figure 11.5 shows the track reconstruction efficiency as a function of transverse momentum and opening angle with the closest neighboring track. The cluster splitting technique (red triangles) recovers 20% of the tracking efficiency at large transverse momenta for which the tracks have neighbors

with opening angles below 5 mrad.

We also performed a study to determine the effects that possible misalignments of the tracker detectors would have on the J/ψ lifetime fits (which determine the fraction of J/ψ mesons coming from B decays). The effect of the various misalignments led to a relative error in the B-fraction ranging from 0.5 to 9% [8].

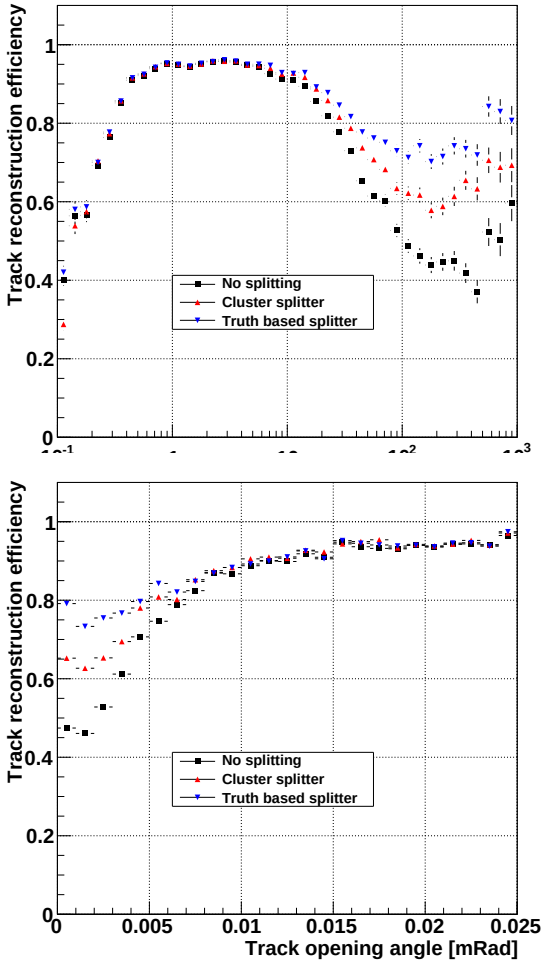

Fig. 11.5 – Track reconstruction efficiency versus transverse momentum for high-p_t jets (top) and of opening angle with the nearest track. The current reconstruction is represented by the black squares; ideal cluster splitting is given by blue triangles while the performance of our splitting algorithm is represented by red triangles.

11.3 Searches for the Higgs boson decaying into $\tau^+\tau^-$

CMS has searched for the neutral Higgs boson[5] decaying into $\tau^+\tau^-$ at $\sqrt{s} = 7$ TeV using 36 pb^{-1} [9]. The reconstructed $\tau^+\tau^-$ mass distribution for leptonic τ decays is shown in Fig. 11.6. There is no evidence for a Higgs boson signal and we set 95% CL upper bounds on the Higgs boson cross section times the τ pair branching fraction. Furthermore, we can interpret the upper limit in the MSSM parameter space given by the mass of the pseudoscalar state, m_A and the ratio of the vacuum expectation values of the two Higgs doublets, $\tan\beta$, for the benchmark scenario m_h^{max} (Fig. 11.7). The present results exclude a region in $\tan\beta$ down to values smaller than those excluded by the Tevatron for $m_A < 140$ GeV/c^2, and significantly extend the excluded region of

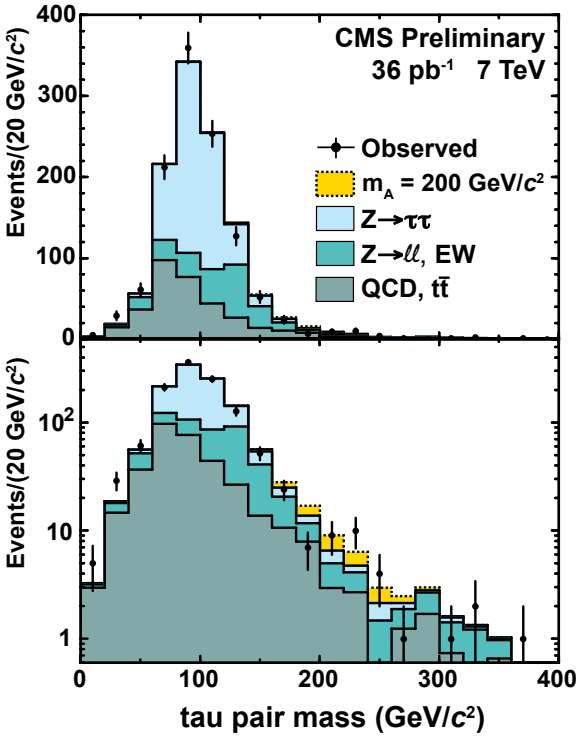

Fig. 11.6 – Reconstructed τ pair invariant mass distribution (linear and logarithmic scales) with the expected backgrounds. The possible contribution from a Higgs boson (m_A =200 GeV/c^2) is shown in yellow.

[5]Minimum Supersymmetric Standard Model (MSSM) Higgs.

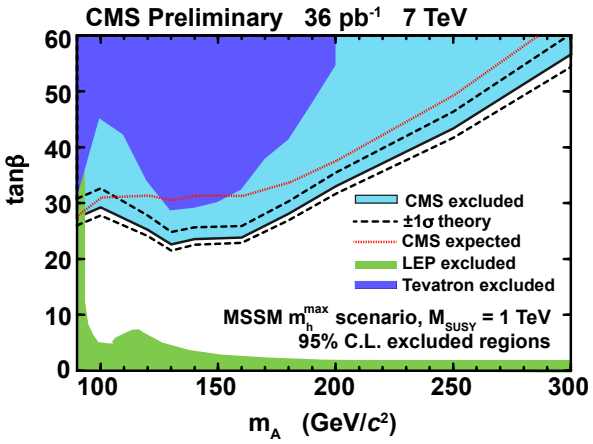

Fig. 11.7 – Regions in parameter space of $\tan\beta$ vs. m_A excluded at 95% CL by CMS, Tevatron and LEP.

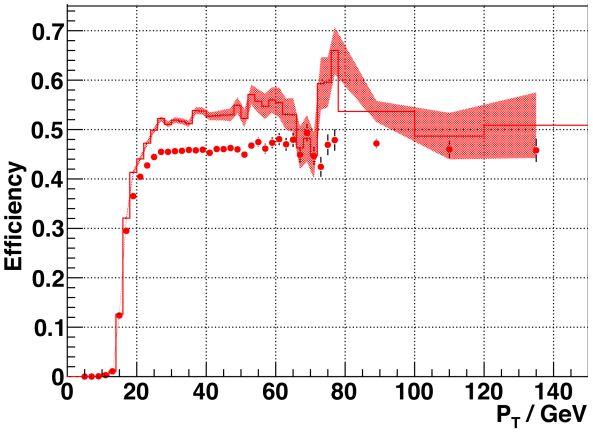

Fig. 11.8 – τ reconstruction efficiency as a function of transverse momentum for two scenarios, corresponding to the 2010 (solid histogram) and 2011 (circles) running conditions.

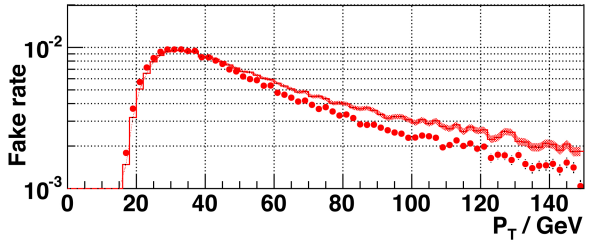

Fig. 11.9 – Fake rate as a function of the τ transverse momentum for 2010 (solid histogram) and 2011 (circles) running conditions.

MSSM parameter space at larger values of m_A.

We are preparing data driven measurements of the τ identification efficiency and studying τ tagging performance using different collision pile-up scenarios. Hadronic τ decays mainly lead to one or three charged pions, with or without neutral pions. The identification algorithm starts with a charged hadron at high transverse momentum, combining with other nearby reconstructed charged hadrons and neutral pions, retaining the combinations consistent with τ decay kinematics. The most isolated one is then selected. Figures 11.8 and 11.9 show the identification efficiency and background contamination from Monte Carlo simulation in two luminosity scenarios for the 2010 and 2011 data taking. A loss of efficiency is observed in 2011 due to the increase in pile-up events. We are optimizing the algorithm to cope with the new running conditions and will soon release an updated Higgs exclusion limit for this channel.

11.4 $B_s \to J/\psi\,\phi$

The decay $B_s \to J/\psi(\to \mu^+\mu^-)\phi(\to K^+K^-)$ is a benchmark channel for CMS for which we have prepared the corresponding software. We are studying this channel to determine the B_s mass and average lifetime of the B_s^H and B_s^L eigenstates. An analysis of the angular correlations can be performed to extract $\Delta\Gamma_s$. Since the expected value for $\Delta\Gamma_s/\Gamma_s$ is small (around 0.2) the mean lives of the two eigenstates are difficult to measure directly from the decay length distribution. However, the two states contribute differently to the angular correlations between the decay particles. We expect to achieve an r.m.s uncertainty of 0.04 on $\Delta\Gamma_s/\Gamma_s$ for an integrated luminosity of about 1 fb^{-1} [10] which should easily be reachable in 2011.

The B_s candidates are selected first with the two-muon trigger, requiring opposite sign muons and reconstructing the J/ψ with a transverse momentum larger than 0.5 GeV/c. The two hadrons (transverse momentum above 0.7 GeV/c) are assumed to be kaons. Their invariant mass is required to be within 10 MeV/c^2 of the known ϕ mass. A

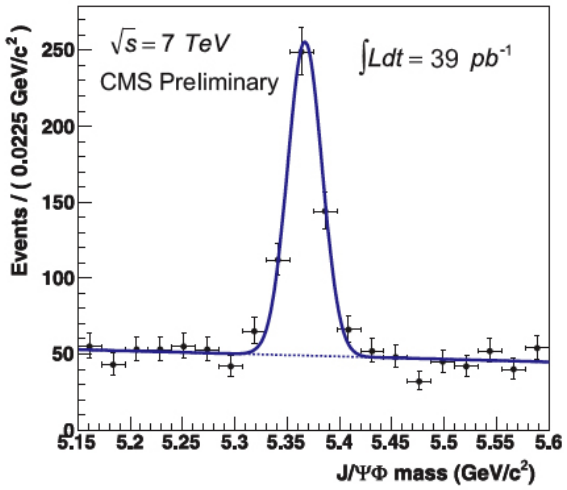

Fig. 11.10 – $(\mu^+\mu)K^+K^-$ invariant mass distribution at $\sqrt{s} = 7$ TeV and $\mathcal{L} = 39$ pb^{-1} showing 377 $\pm$ 26 B_s decays.

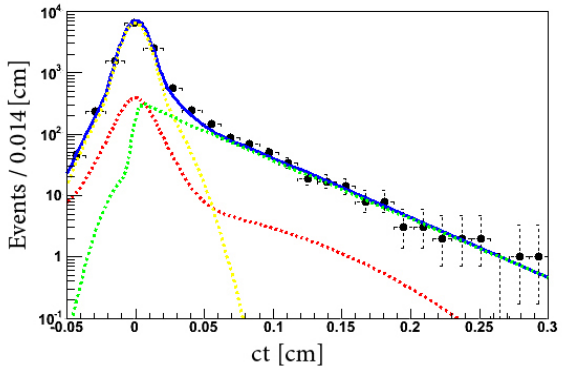

Fig. 11.11 – Decay length distribution with likelihood fit. Red: background; yellow: prompt background; green: signal; blue: total.

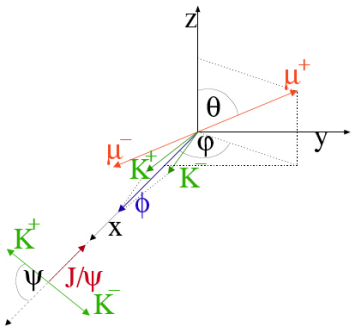

Fig. 11.12 – Definition of the angles θ, ϕ and ψ that describe $B_s \to J/\psi\ \phi$ decay.

kinematic fit constraining the J/ψ mass and a cut on the B_s decay length ($c\tau/\sigma > 3$) are then applied. Figure 11.10 shows the B_s with an integrated luminosity of 39 pb^{-1}, obtained by CMS at 7 TeV. The fitted mass is 5367.0 $\pm$ 1.2 MeV (compared to the PDG value of 5366.3 $\pm$ 0.6 MeV [11]). Figure 11.11 shows the decay length distribution for the B_s. A two-dimensional likelihood fit was applied. The result from the fit is $c\tau$ = 454.6 $\pm$ 15.8 μm (compared to the PDG value of 425.0 $\pm$ 12.6 μm).

Figure 11.13 shows our preliminary distributions for the angles θ, ϕ and ψ (defined in Fig. 11.12) for the data collected so far in 2010 and 2011. The similarities with Monte Carlo simulation using the decay parameters from ref. [10] are quite encouraging.

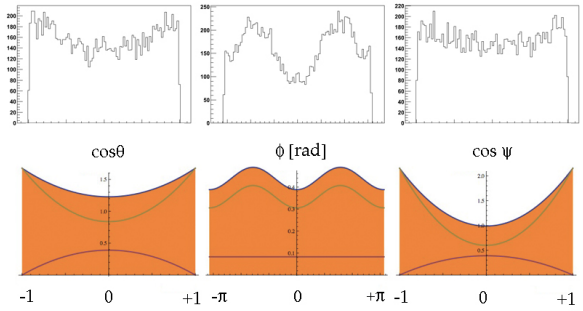

Fig. 11.13 – Top: Measured distributions of $\cos\theta$, ϕ and $\cos\psi$ obtained with 46 pb^{-1} at 7 TeV. Bottom: Predictions for CP-odd (pink) and CP-even (green) B_s-states [10].

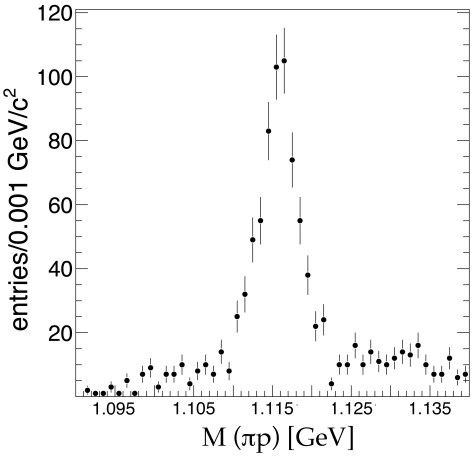

Fig. 11.14 – πp invariant mass distribution showing the Λ ($\bar{\Lambda}$).

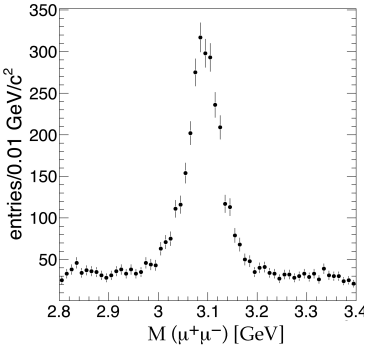

Fig. 11.15 – $\mu^+\mu^-$ invariant mass distribution showing the J/ψ.

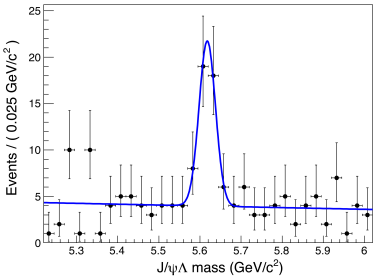

Fig. 11.16 – $J/\psi\Lambda$ invariant mass distribution with 40 pb^{-1} of data (36 ± 9 events) with Λ_b fit (blue line).

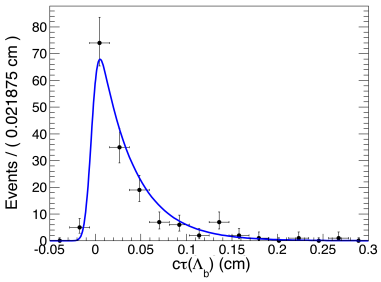

Fig. 11.17 – Λ_b proper decay length distribution.

11.5 Study of b–baryons

The spectroscopy of heavy baryons is of interest to QCD and to models of the strong interaction [12]. The quark model predicts 56 heavy ground state baryons (with at least one c or b-quark). So far only 8 b-baryons have been observed, but the evidence often rests on a handful to a few dozen events.

The study of heavy baryons by our group was launched with a study of the neutral Λ_b (udb). The decay channel $\Lambda_b \to J/\psi\ \Lambda$ with $J/\psi \to \mu^+\mu^-$ and $\Lambda \to \pi^- p$ can be studied at CMS. Both Λ_b and Λ are long-lived particles, traveling up to several centimeters before decaying (leading to displaced vertices), and muons in the final state which can be triggered on. The Λ (Fig. 11.14) is combined with the $J/\psi \to \mu^+\mu^-$ (Fig. 11.15) to form Λ_b candidates. Distributions of invariant mass and proper decay length of the Λ_b are shown in Figs. 11.16 and 11.17, respectively.

These data were collected in 2010 with an integrated luminosity of 40 pb^{-1}. A clear Λ_b mass peak is observed after applying a series of cuts (e.g. reasonably large transverse momenta and proper decay length $c\tau(\Lambda) > 1$ cm, $c\tau(\Lambda_b) > 50$ μm). A maximum likelihood fit was performed with a single Gaussian plus a linear background for the mass distribution, and a Gaussian plus exponential function for the proper decay length. We obtain $M(\Lambda_b) = 5618 \pm 5$ MeV and $c\tau(\Lambda_b) = 379 \pm 33$ μm (statistical errors only) in agreement with the known values (5620.2 ± 1.6 MeV, resp. 417 ± 11 μm [11]).

The reconstructed Λ_b candidates are a starting point to search for further heavy baryons, the $\Sigma_b^{(*)+}$ (uub) and $\Sigma_b^{(*)-}$ (ddb). The dominant decay mode is $\Sigma_b \to \Lambda_b\pi$, a strong decay that takes place at the primary vertex. The selection of the soft pion coming from Σ_b is not easy in the dense environment around the primary vertex. Apply-

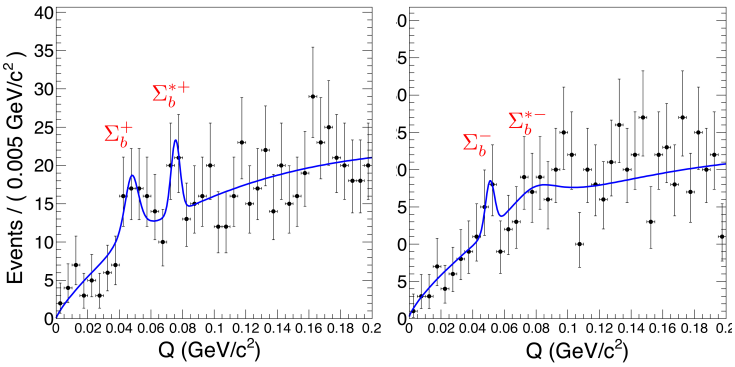

Fig. 11.18 – Q-value distribution for $\Sigma_b \to \Lambda_b\pi$ for positive (left) and negative (right) charges from the first 40 pb^{-1} of data. The blue line shows a simultaneous maximum likelihood fit.

ing loose cuts in view of the still limited statistics, and combining each Λ_b candidate with an extra track, leads to four potential peaks from Σ_b states. Figure 11.18 shows the reconstructed Q-value distribution of the decay $\Sigma_b \rightarrow \Lambda_b\pi$ where $Q = M(\Lambda_b\pi) - M(\Lambda_b) - M(\pi)$. The theoretically predicted Q-values lie in the range 0.03 – 0.1 GeV [13]. A simultaneous maximum likelihood fit was applied with a smooth function to parameterize the background and a Breit-Wigner distribution convoluted with a Gaussian for each mass peak. Equidistance between the peak mean values were required. Our preliminary measurements are in agreement with theoretical expectations and the measurements by CDF [14]. These early indications of signals from the very first and limited LHC data make the study of b-baryons very promising.

Triggers specific to particular processes will be needed as the luminosity increases. CMS reconstructs b-hadrons through their decay into a $J/\psi \rightarrow \mu^+\mu^-$. Triggering on J/ψ is achieved with the high level trigger on $\mu^+\mu^-$ and the additional requirement that the J/ψ should be emitted from a secondary vertex. However, many channels such as $\Lambda_b \rightarrow J/\psi(\rightarrow \mu^+\mu-)\Lambda(\rightarrow p^+\pi^-)$, $\Xi_b^- \rightarrow J/\psi(\rightarrow \mu^+\mu-)\Xi^-(\rightarrow \Lambda\pi^-)$, $\Omega_b^- \rightarrow J/\psi(\rightarrow \mu^+\mu-)\Omega^-(\rightarrow \Lambda K^-)$ have long-lived particles leading to tertiary vertices far away from the J/ψ vertex, often beyond the pixel detector. The straightforward approach is to select high transverse momentum tracks (proton from Λ decay) with large impact parameter with respect to the secondary and primary vertices. A second lower transverse momentum track (e.g. pion from Λ decay) is then required. This work is in progress.

11.6 b-jet tagging

Identifying jets containing b-decays ("b-tagging") is an essential tool for a wide range of topics in and beyond the Standard Model [15]. In CMS b-tagging tools have been applied in e.g. measurements of the inclusive b- and t-quark production cross-sections.

We have been involved in b-tagging since many years with one of us (A.S.) coordinating the commissioning of b-jet identification with 7 TeV collision data [16]. The crucial device for good b-tagging performance is the pixel detector which reconstructs charged tracks close to the proton-proton interaction point. One of the most important quantities is the impact parameter (IP),

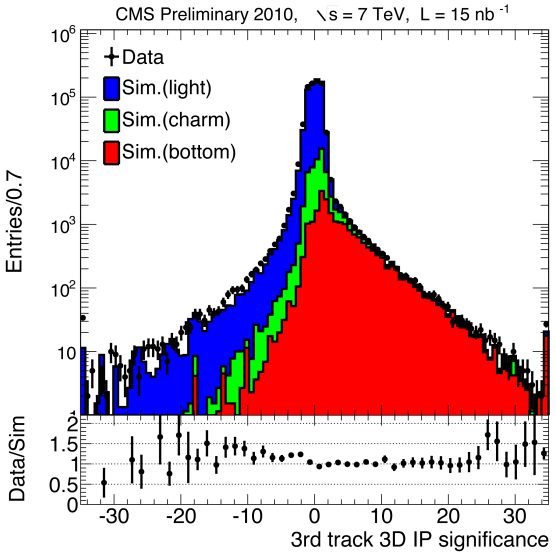

Fig. 11.19 – Impact parameter (IP) significance of the third track in a jet (ordered by IP significance) compared to simulation results for light, charm and jets.

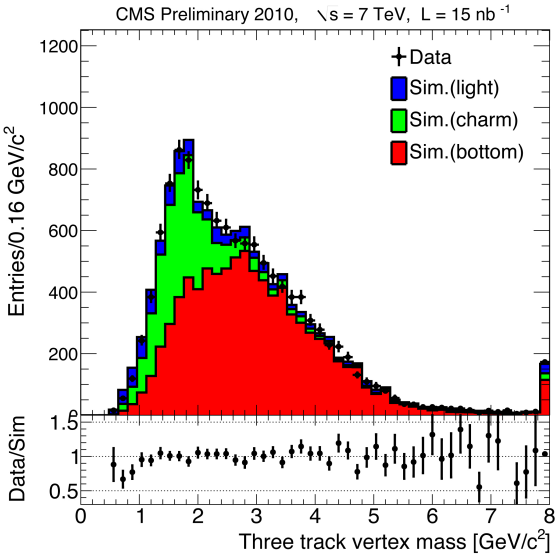

Fig. 11.20 – Invariant mass of secondary vertices with at least three tracks compared to simulation results.

the distance of closest approach of a trajectory to the proton-proton interaction vertex. The IP significance of the third track in a jet is shown in Fig. 11.19. The tail in this distribution is quite sensitive to b-quarks, and is therefore used as discriminator in a high purity b-tagging algorithm. The secondary vertex from B decays can be reconstructed using the so-called adaptive vertex fitting technique [17]. A secondary vertex with three or more tracks has a high probability of being a B decay vertex. The flight distance which is defined as the separation between the primary and secondary vertices is used in the b-tagging algorithm.

Another important quantity is the invariant mass of the secondary vertex, assuming pions. This quantity is shown in Fig. 11.20 for vertices with three or more tracks. With the vertex mass one can distinguish between light flavours, charm and beauty. This was used in the measurement of the inclusive b production cross-section [18], the first precision measurement using b-tagging in CMS. First results on performance in b-tagging have been published [16] but systematic errors are still large. Our group continues to play a leading role in the b-tagging group in 2011.

In parallel with CMS studies of the inclusive cross-section for $pp \rightarrow b + X$ we contributed to the study of the angular correlation between pairs of B mesons. We have enhanced the performance of the b-tagging algorithm to reconstruct two b-jets with close spacial separation. We select events with one secondary vertex each which have similar spatial coordinates (distance smaller than typically 20μm), mix them pairwise and reconstruct them. Events for which both initial secondary vertices are reconstructed in the mixed events are then counted. The efficiency of the vertex finder is calculated as the fraction of the number of secondary vertices in the mixed sample to the corresponding number in both event samples before mixing. The efficiency was studied as a function of vertex separation ΔR, defined as $\sqrt{\Delta\eta^2 + \Delta\phi^2}$, where η is the pseudorapidity and ϕ the azimuthal angle.

On the other hand, we have predicted the fraction of b-quarks produced collinearly or not, that is via gluon-splitting or through flavor creation/excitation, respectively. This study, made with `Pythia` and `Madgraph`, led to a first estimate of the relative importance of the "gluon splitting" peak compared to the back-to-back region mainly due to flavor creation or excitation. This was calculated for different p_T ranges of the leading jet (Fig. 11.21. The ΔR dependence of the double vertex reconstruction efficiency (Fig. 11.22) shows very good agreement for the shape between data and simulation, with discrepancies below 2% [19]. Efficiencies of typically 90% for the double vertex reconstruction can be reached.

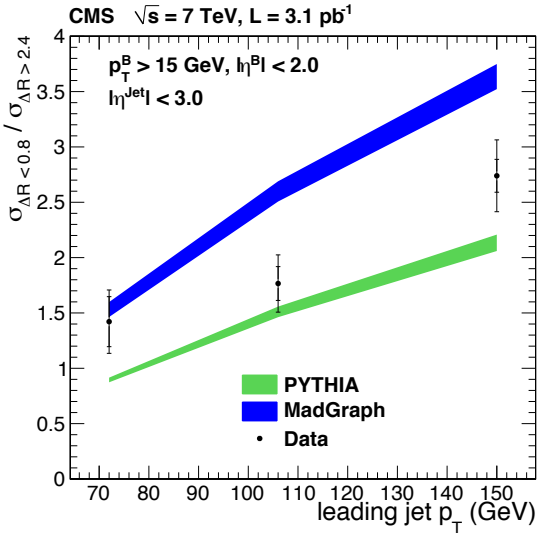

Fig. 11.21 – Ratio between the gluon splitting region (ΔR <0.8) and the back-to-back region (ΔR >2.4) for three values of the p_T cut.

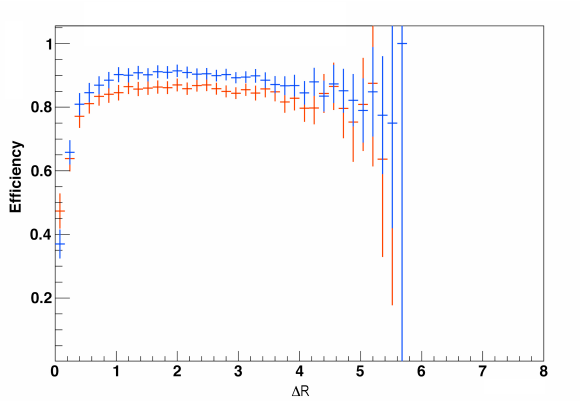

Fig. 11.22 – Double vertex reconstruction efficiency as a function of ΔR for a vertex separation of 20 μm. The data are shown in red, the simulation in blue.

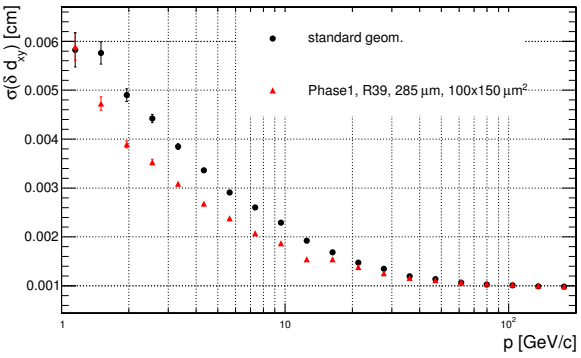

Fig. 11.23 – Transverse impact parameter resolution versus number of tracks at a luminosity of 10^{34} $cm^{-2}s^{-1}$, before and after the upgrade.

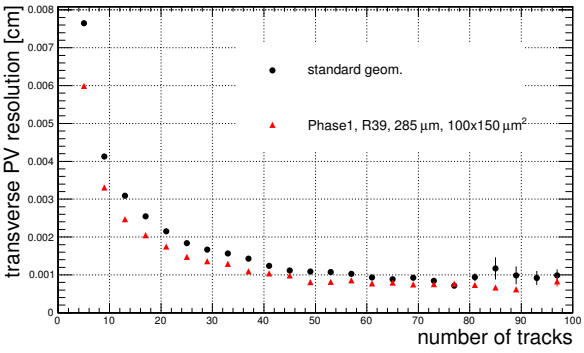

Fig. 11.24 – Transverse primary vertex position resolution as a function of the number of tracks.

11.7 Preparations for the pixel detector upgrade

The pixel system will be replaced in 2016 – 2017 during the "Phase 1" luminosity upgrade. Major modifications to the detector layout and to the readout electronics will be needed to prevent data losses and to provide sufficiently good performance in hit and track reconstruction. The new detector will include an additional fourth barrel layer and one disk in each endcap section. The passive material will be reduced by up to a factor of two in the central tracking region, thanks to the new readout electronics and evaporative cooling technique. Adopting the 0.13 μm CMOS technology for the front-end chip in the innermost layers is currently under evaluation.

We have assessed the performance of the upgraded detector [20]. For the transverse impact parameter resolution the expected enhancement is about 25% in the barrel (Fig. 11.23) and up to 40% in the endcaps. The transverse primary vertex resolution will improve by about 20% (Fig. 11.24). A 20% improvement is expected on decay vertices from b-hadrons. A replacement of the innermost sensors will be required after the high luminosity run. Up to 50% improvement in spatial resolution and reconstruction performance was estimated with thinner sensors with smaller pixel cells (75×100 μm^2).

Data taking with CMS resumed in March 2011 and will continue during 2012, with a short break during the winter holidays. The LHC luminosity in 2011 already exceeded 3.5×10^{32} $cm^{-2}s^{-1}$, surpassing the values from 2010. The expected integrated luminosity 2011/12 is several fb^{-1}. The machine should be able to reach the design center-of-mass energy of $\sqrt{s} = 14$ TeV after the 2013 – 2014 shutdown.

[1] S. Chatrchyan *et al.* [CMS Collaboration], Journal of Instrumentation **3** (2008) S08004.

[2] Y. Allkofer *et al.*, Nucl. Instr. Meth. in Phys. Research **A 584** (2008) 2.

[3] V. Chiochia *et al.*, Nucl. Instr. Meth. in Phys. Research **A 568** (2006) 51.

[4] A. Schmidt *et al.*, Journal of Instrumentation **4** (2009) P05003.

[5] V. Khachatryan *et al.* [CMS Collaboration], JHEP **1103** (2011) 136.

[6] V. Khachatryan *et al.* [CMS Collaboration], Eur. Phys. J. C **70** (2010) 1165.

[7] M. Swartz, Nucl. Instrum. Meth. **A 511** (2003) 88.

[8] V. Khachatryan *et al.* [CMS Collaboration], Eur. Phys. J. **C 71** (2011) 1575.

[9] V. Khachatryan *et al.* [CMS Collaboration], CMS-PAS-HIG-10-002.

[10] L. Wilke, PhD-Thesis, University of Zurich (2009).

[11] K. Nakamura *et al.* (Particle Data Group) J. Phys. G: Nucl. Part. Phys. **37** (2010) 075021.

[12] E. Klempt and J.-M. Richard, Rev. Mod. Phys. **82** (2010) 1095.

[13] W.Y.P. Hwang and D.B. Lichtenberg, Phys. Rev. **D 35** (1987) 3526.

[14] T. Aaltonen *et al.*, Phys. Rev. Lett. **99** (2007) 202001.

[15] A. Schmidt, Proceedings of Science (EPS-HEP 2009) 439.

[16] The CMS Collaboration, CMS Physics Analysis Summary BTV-10-001 (2010).

[17] R. Fruewirth, W. Waltenberger, and P. Vanlaer, CMS Note 2007/008 (2007).

[18] The CMS Collaboration, CMS Physics Analysis Summary BPH-10-009 (2010).

[19] CMS collaboration, submitted to J. of High Energy Phys.

[20] C. Favaro, Nucl. Instrum. Meth in Phys. Research **A** (in print).